Ablation with a Large Fraction of Solid Removal

George Y. Jumper Jr.*
Worcester Polytechnic Institute, Worcester, Massachusetts
and
James E. Hitchcock†
Air Force Institute of Technology, Wright-Patterson Air Force Base, Ohio

Experiments were performed comparing the ablation performance of a pure subliming substance to a substance with a large fraction of nonsubliming material. The subliming substance was solid carbon dioxide. Models with a large fraction of nonsubliming material were a composite of carbon dioxide and glass beads. The performance of the pure substance compared very favorably to theory. The composite models experienced a reduction in stagnation-point carbon dioxide mass loss and a departure from the predicted mass-transfer profile around the body. A more complete theoretical model of the composite surface helped explain the reduced stagnation-point mass flux.

Nomenclature

B' = mass-addition parameter [Eq. (6)]
C_H = Stanton number
C_{Ho} = Stanton number without mass addition
D = binary diffusion coefficient
F_D = fraction of surface available for diffusion
F_S = fraction of surface available for sublimation
h = enthalpy
K = mass fraction of specie in gas phase
k = thermal conductivity
ℓ = depth of diffusion well
Le = Lewis number
M = molecular weight
$\dot{m}$ = mass flux of subliming material
$\dot{m}^*$ = mass flux of nonsubliming material
P = mixture pressure
p = partial pressure
q = heat flux
R = universal gas constant
T = temperature
u = streamwise velocity
v = velocity normal to surface
X = energy parameters [Eq. (10)]
y = coordinate normal to the surface
α = vaporization coefficient
Δh = change in enthalpy
ρ = density

Subscripts

e = edge of boundary layer
eq = equilibrium
i = index for summation
int = to the interior
r = recovery or adiabatic wall
rad = radiative
s = at the subliming surface
T = total
sub = sublimation
w = fluid dynamic wall
1 = subliming specie
2 = "air"

Superscript

* = nonsubliming material

Presented as Paper 86-1260 at the AIAA/ASME 4th Joint Thermophysics and Heat Transfer Conference, Boston, MA, June 2–4, 1986; received June 5, 1986; revision received Sept. 30, 1987.

*Associate Professor, Mechanical Engineering Department. Member AIAA.
†Professor, Department of Aeronautics and Astronautics.

Introduction

THERMAL protection by ablation is often used in environments in which direct observation is extremely difficult. Typical applications include the protection of rocket nozzle throats and reentry vehicle nose tips and sidewalls. The lack of definitive data has hampered attempts to model these events that are described by coupled theories from aerodynamics, heat transfer, and material science. At best, the researcher is forced to simulate small parts of the problem to help validate the overall model.

This particular study was prompted by abnormally high mass loss rates of graphite reentry vehicle nose tips. A popular hypothesis was that the anomaly was caused by substantial removal of the ablator in the solid phase along with the expected removal in the vapor phase. It was postulated that the ratio of solid-phase to vapor-phase removal for graphite could exceed one.[1,2] Although the estimated mechanical loss fraction was revised downward, uncertainties remained since it was never possible to measure directly the fraction of solids removed from the ablating graphite surface. The applicability of this study extends beyond the graphite problem. Since solid removal can be a potential problem in the severe environmental conditions associated with ablative thermal protection, it is important to understand the effects of solid removal on the thermochemical process. In addition, there may be applications, such as signature alteration, when controlled solid release might be desirable.

The purpose of this study was to compare the ablation performance of a pure subliming material to that of an ablative material with a known amount of nonsubliming material, and to compare the experimental data with theoretical models. The ablative material was solid carbon dioxide (dry ice) and the nonsubliming material was glass beads.

Simple Theory

In order to define the experiment, the authors extended the theory described by Kubota[4] to include solid removal. The mass and energy fluxes are shown schematically in Figs. 1 and 2. The coordinate system is fixed to the solid-gas interface. The

system is assumed to have only three nonreacting components: the subliming substance, the surrounding gas ("air"), and the nonsubliming component of the ablative material.

Partition the solid mass flux into two parts: $\dot{m}$, the part that sublimes, and $\dot{m}^*$, the part that does not. The conservation of mass equation for the subliming specie is

$$(\rho v)_w K_w - \left(\rho D \frac{\partial K}{\partial y}\right)_w = \dot{m} \tag{1}$$

When combined with the conservation of mass equation for the air, the resulting convective mass flux is

$$(\rho v)_w = \dot{m} \tag{2}$$

The conservation of energy equation for the system is

$$(\dot{q}_{\text{rad}})_{\text{net}} - \left(k \frac{\partial T}{\partial y}\right)_w - \sum_{i=1}^{2} \left(\rho D h_i \frac{\partial K_i}{\partial y}\right)_w + \dot{m}^* h_w^* + (\rho v h)_w + \dot{q}_{\text{int}} = \dot{m} h_s + \dot{m}^* h_s^* \tag{3}$$

Since there is no phase change associated with the nonsubliming specie, and assuming that the temperature of the nonsubliming specie does not change across the interface, the h^* terms are equal and cancel out. The resulting equations are the same as those used by Kubota in his analysis. Kubota's results can be directly applied to the system, provided that the mass-flux term is interpreted as the mass flux of the subliming material only. Stated another way, the presence of nonsubliming material should not change the subliming mass flux and wall temperature predicted by conventional thermochemical theory.

Following Kubota, it is assumed that internal heat conduction and net radiative heat transfer to the surface are negligible, the Prandtl and Lewis numbers are unity, and there is binary diffusion in the gas phase, which is assumed to be a mixture of two ideal gasses. With these assumptions Eqs. (1) and (3) reduce to

$$B' = \frac{M_1}{M_2} \frac{p_{1w}}{P - p_{1w}} \tag{4}$$

$$B' = \frac{h_r - h_{2w}}{\Delta h_{\text{sub}}} \tag{5}$$

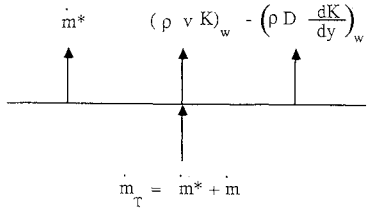

Fig. 1 Mass flux of ablating species through surface.

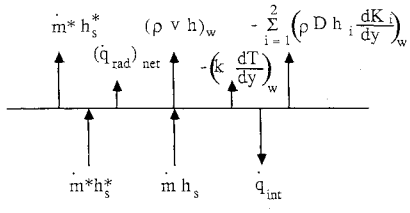

Fig. 2 Energy flux through surface.

where B' is the nondimensional mass-transfer coefficient defined by the equation

$$B' = \frac{\dot{m}}{\rho_e u_e C_H} \tag{6}$$

If the vapor of the subliming specie is assumed to be in equilibrium with the solid phase, the partial pressure is the equilibrium vapor pressure, which is a function of the wall temperature. Given boundary-layer edge conditions P and h_r, the vapor pressure vs temperature relationship, and the enthalpy of sublimation for the material, Eqs. (4) and (5) can be solved for a unique B' and wall temperature.

Mass flux is calculated using Eq. (6), which requires the calculation of the Stanton number. Standard convective heat-transfer analysis techniques can be used to calculate the Stanton number without any mass transfer from the surface C_{Ho}. Two corrections should be applied. Kubota recommends the correction of Gazley et al.[5] for the reduction of heat transfer due to mass addition to the boundary layer. Kays[6] recommends that the heat transfer Stanton number be modified with a Lewis number correction when applying it to mass-transfer problems. With these corrections the mass flux is computed by the following equation:

$$\dot{m} = (\rho_e u_e C_{Ho}) \left[1 + 0.64 \left(\frac{M_2}{M_1}\right)^{1/3} B'\right] (Le^{2/3}) B' \tag{7}$$

Experimental Conditions

The primary goal in the design of the experiment was to select conditions and materials that could be carefully controlled and measured in order to predict accurately the heat and mass transfer. To have a reasonable hope of extrapolating the results to graphite under reentry conditions, the value of B' should be a minimum of 0.1, the value associated with the oxidation-controlled regime of graphite,[3] and the size of the nonsubliming material should be approximately equal to the stagnation-point boundary-layer thickness.[1] After surveying the available facilities, equipment, and low-temperature subliming materials, the following experiment evolved.

A low-turbulence subsonic free-jet[7] facility was used. The free jet afforded open access to the model and elminated the problem of recirculation of the solid particles. The conditions of the jet were ambient pressure and near 273 K temperature. With these environmental conditions solid carbon dioxide was the best subliming material. The resulting B' was slightly less than 0.2. The model geometry selected was a hemispherical forebody of 25 mm diam on a cylindrical afterbody. Axisymmetrical flow was chosen over a two-dimensional flow configuration for a more accurate determination of the shape change during the experiment. The potential flow solution for the selected shape is one of the many computed by Smith and Pierce,[8] who showed that the edge velocity distribution merges into that of a sphere near the stagnation point. The initial stagnation-point heat transfer for this geometry is identical to that of a sphere.

The experiment was performed at Mach numbers below 0.1 that further simplified the prediction of the ablation response.

Table 1 Comparison of BLIMP and the simple theory

	BLIMP	Simple	Difference, %
T_w, K	181	172	−5.0
B'	0.193	0.192	−0.5
$\rho_e u_e C_{Ho}$, kg/m²·s	0.262	0.268	2.3
C_{Ho}/C_H	1.094	1.107	0.9
$\rho_e u_e C_H$, kg/m²·s	0.239	0.242	1.3
$\dot{m}$	0.0461	0.0465	0.9

The pressure did not significantly vary around the body and the recovery air temperature was essentially constant and equal to the freestream air temperature. With these conditions the simple theory predicts constant wall temperature and B', which further implies a constant ratio of C_H to C_{Ho}. The mass loss is then directly proportional to the heat-transfer coefficient around the body.

Improved Theoretical Prediction

With the experimental conditions selected, an improved analysis was performed to check the simple theory. The problem was run using the boundary layer integral matrix procedure (BLIMP) written by Bartlett and Kendall.[9] The solution provided a mass-transfer prediction for the entire hemispherical forebody and takes into account the individual air species and unequal diffusion coefficients. A laminar boundary layer was assumed and the program was run in the "quasisteady" mode. BLIMP includes mass addition directly in the solution, and so it would not normally provide information concerning the ratio of heat transfer with and without mass addition. This information was deduced by rerunning BLIMP without mass addition using the wall temperatures predicted in the mass addition case. The comparison of BLIMP to the simple theory is shown in Table 1. The agreement is an excellent endorsement of the accuracy of the simple theory. The largest disagreement is the 5% error in predicted wall temperature. This was later attributed to the fact that the carbon dioxide equilibrium vapor pressure-temperature correlation was not optimized for the temperature range of interest. BLIMP confirmed the assumption that B' and wall temperature were approximately constant around the surface. The predicted temperature variation was 0.11 K (0.065%) and B' variation was 0.0015 (0.78%). The calculation predicted the expected mass-transfer distribution around the hemispherical forebody that is shown in Figs. 6 and 7 with the experimental results.

Ablation Models

The 25-mm-diam models were produced in molds made of seamless tubing with a hemispherical end-plug. The molds had a single fitting opposite the hemispherical end to introduce the carbon dioxide into the mold. A plastic rod was frozen into the center of each model to serve as a solid attachment point. The rod had a hole drilled along the axis so that a thermocouple junction could be placed near the center of the hemispherical nose.

Mixed solid-vapor removal was achieved by dispersing glass beads in the carbon dioxide. The bead size closest to the boundary-layer thickness of this experiment was 120 μm diam. The beads were screened to improve size uniformity. The bead shape was reasonably spherical. Initial attempts to compress mixtures of glass beads and dry ice "snow" were abandoned due to difficulties in achieving uniform bead distribution and uniform dry ice density. A uniform composite of maximum glass bead fraction was produced by fully packing the molds with glass beads before introduction of the dry ice. The experiments served as a comparison of the two extremes: no solid removal for the pure dry ice models and massive solid removal for the fully packed models.

The production technique proceeded as follows. The mold was filled with preheated beads, then maintained at 360 K in an oven for at least 1 h to eliminate moisture. The hot mold was then attached to the carbon dioxide filling system that is shown in Fig. 3. A vacuum pump attached to the fixture maintained a very low pressure in the mold while it was cooling. When cool, the mold was placed in an insulated container and surrounded by commercially supplied dry ice. The system was then pressurized with carbon dioxide to well above the triple point pressure of 0.51 MPa (typically 1.5 MPa) to insure that the carbon dioxide would condense in the mold, flow down through the glass beads in the liquid phase, then finally solidify when sufficient

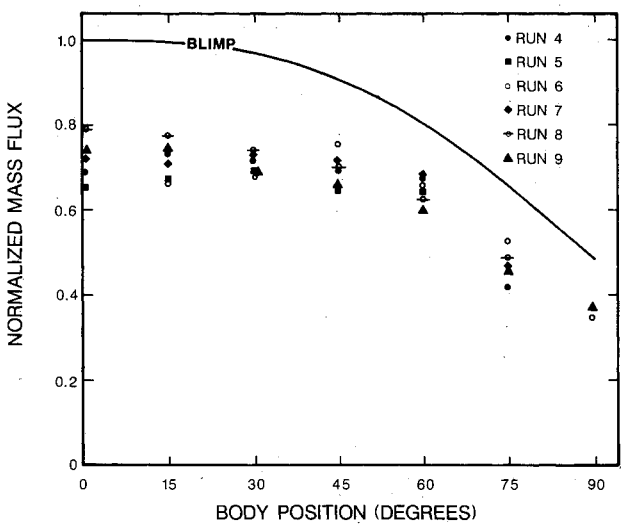

Fig. 4 Typical set of recession profiles for pure carbon dioxide models.

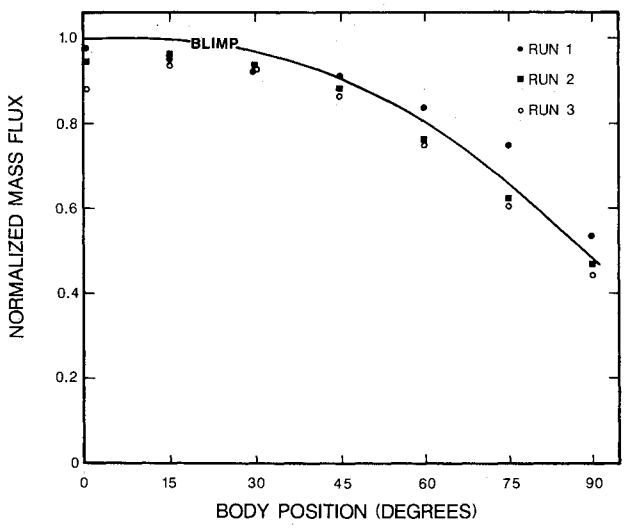

Fig. 3 System for producing ablation models.

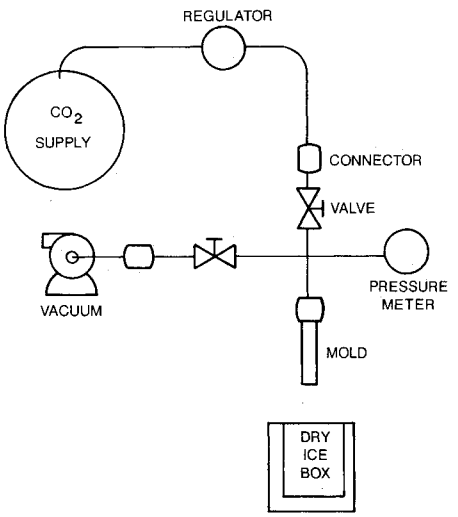

Fig. 5 Typical set of recession profiles for composite models.

Table 2 Physical properties

Prandtl number[a]	0.735		
Lewis number[a]	0.886		
Schmidt number[a]	0.829		
Solid properties at 170 K	Carbon dioxide	Glass	Composite
Density, Mg/m^3	1.60(10)[b]	2.45	2.09
Thermal conductivity, W/m·K	0.71(14)	0.79(15)	0.71
Specific heat, kJ/kg·K	1.2(10)	0.84(15)	0.92
Thermal diffusivity, mm^2/s	0.38	0.38	0.38
Mass fraction in composite	0.29	0.71	
Volume fraction	0.39	0.61	
Carbon dioxide properties			
Enthalpy of sublimation, kJ/kg	589.1 (14)		
Vapor pressure[c] (atm) $\text{Log}_{10}(p) = -1352.4/T + 6.9576$			

[a]At Eckert's reference temperature (approximately 222 K).[15] [b]Number in parenthesis is the reference number. [c]This correlation is based on the enthalpy of sublimation at 170 K and the vapor pressure data reported in Ref. 14.

carbon dioxide was in the mold. The high pressure was maintained for several hours, typically overnight, then the regulator was closed. Within 5 h the pressure in the mold decreased to slightly above atmospheric pressure as the remaining vapor solidified. The filling procedure was reasonably successful. Only a small fraction of the models had pockets of glass beads that had not been completely encased in carbon dioxide.

Overall model integrity was not very encouraging. Of approximately 30 models constructed, only 12 were good enough to warrant full wind-tunnel tests. Of those 12, only nine yielded good symmetrical shape change data. The most prevalent problem was breakage upon removal from the molds. The composite models were the strongest and most reliable. The pure carbon dioxide models were clear, with a very visible grain structure of approximately 10 mm from boundary to boundary. The models tended to fracture along the boundaries. Even those that did not fracture often experienced preferential ablation along the grain boundaries.

The Test Facility

A free jet, built for an Air Force Institute of Technology aeroacoustic study,[7] supplied dry, very low-turbulence air to the models. The jet exit was 102 × 76 mm. The model size and placement were consistent with aerodynamic testing standards required to simulate free flight through still air. Model shape as a function of time was obtained from 35-mm photographs of the model. A stopwatch and a reference scale were also in the field of view. The models were photographed against a flat black background. They were front lighted by a strobe flash attached to the camera. With a 270-mm telephoto lens the camera could be positioned about 2 m from the model to minimize parallax.

Data Reduction

All of the data required to determine surface recession rate were contained on the 35-mm film. Each frame was projected onto the light table of a precision film reader. The distance reference and nozzle exit plane were used for frame-to-frame alignment. Each surface profile was traced and the time was recorded. Typical recession profiles for the pure models are shown in Fig. 4 and for the composite models in Fig. 5. The 13-ray reference is an overlay that was positioned at the center of curvature of the earliest picture. The rays are 15 deg apart.

The conversion from recession profile to local recession rate was accomplished by digitizing the surface location points along each ray, plotting them versus time, then performing a least squares linear through points of interest. The stagnation-point recession for pure carbon dioxide models was surprisingly constant, which is attributed to the compensating influences of reducing model diameter and increasing nose

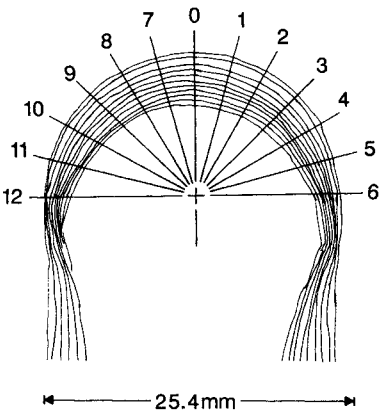

Fig. 6 Experimental carbon dioxide mass loss from pure substance models compared to theoretical predictions (all data normalized by the predicted stagnation-point mass loss).

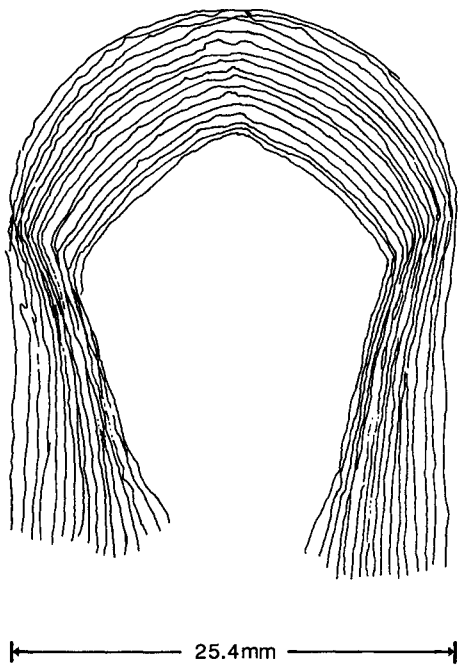

Fig. 7 Experimental carbon dioxide mass loss from composite models compared to theoretical prediction for pure substance (all data normalized by the predicted stagnation-point mass loss).

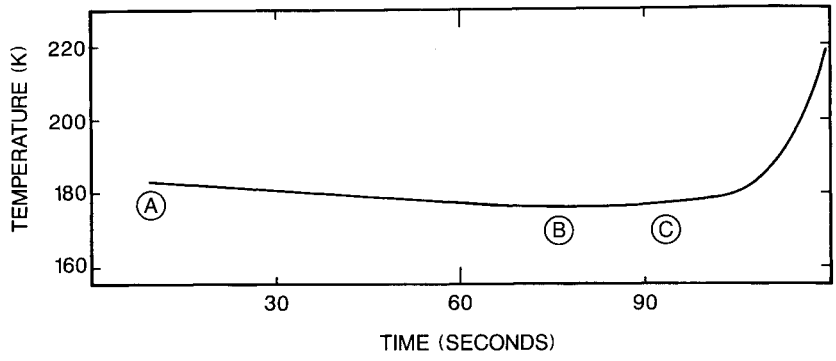

Fig. 8 Typical internal temperature record.

bluntness. The composite-model recession maintained an initial rate associated with the hemispherical shape for approximately 60 s, then transitioned to a lower rate as the model become more conically shaped.

Physical Properties

The physical properties of the experimental materials are listed in Table 2. The composite thermal properties are based on the properties of the constituents. Since the conductivities of the materials are nearly identical, the effective conductivity of the composite is essentially that of the continuous phase.[11] The specific heat of the composite is the mass weighted average of the two constituents.

In order to obtain the carbon dioxide mass loss rate, the linear recession rate is multiplied by the density of the carbon dioxide. The density of pure carbon dioxide in the temperature range of interest was determined by Maass and Barnes[10] to be 1.60 Mg/m^3. By preparing some special gravimetric samples, it was determined that the density of the glass beads in the composite models was 1.48 ± 0.02 Mg/m^3 of the composite, and the density of the composite itself was 2.09 ± 0.03 Mg/m^3. Consequently, the density of the carbon dioxide in the composite was 0.61 ± 0.05 Mg/m^3. This is in close agreement with the result predicted using the density of pure glass and the volume fractions shown in Table 2 that were determined in a gravimetric experiment using water and glass beads. The glass-bead volume fraction of 61% is somewhat lower than the theoretical maximum near 68%, but well within reasonable bounds considering actual sphericity and typical packing efficiencies.[16]

Experimental Run Conditions and Results

The conditions and results for each run are listed in Table 3. The mass loss results for the pure carbon dioxide models are summarized in Fig. 6. The data have been normalized by the stagnation-point mass flux predicted by BLIMP, adjusted to the particular conditions of the experiment by the simplified theory. The normalized mass-transfer rate around the body as predicted by BLIMP is also shown. Except for the stagnation-point value, each data point shown is the average of the values on either side of the stagnation point. The results are in fair agreement with the predicted results, generally falling below the prediction. The stagnation-point mass flux is 6.5% below the prediction.

The normalized carbon dioxide mass-transfer results of the composite models are shown in Fig. 7. The average stagnation-point mass loss rate was 28% less than the amount predicted by the approximate theory, or 23% less than the experimentally observed rates of the pure carbon dioxide models. The mass loss data for these models also exhibited more scatter.

A typical internal-temperature history is shown in Fig. 8. Referring to the labels on that figure, the response can be divided into three periods, 1) of decreasing temperature (A to B), 2) of approximately constant temperature (B to C), and 3) of increasing temperature (C to the end of the test). The initial temperature drop is an indication that the temperature of the dry-ice-packed container in which the model was formed was warmer than the equilibrium wall temperature during the convective heat and mass-transfer process. The approximately constant temperature, referred to as the asymptotic temperature, was interpreted as the equilibrium wall temperature. Of three experiments with pure carbon dioxide, the mean asymptotic value was 179.3 K. Of 10 experiments with composite models the mean asymptotic value was 182.1 K. The increasing temperature period is an indication of thermocouple exposure to the warmth of the airstream.

Comparison of Theoretical and Experimental Results

In contradiction to the simple theory for solid removal, the presence of glass beads did reduce the carbon dioxide mass flux

Table 3 Experimental run conditions and results

	Air			Model	Predicted			Experimental		
Run	Temp, K	Press, kPa	Velocity, m/s	radius, mm	B', n.d.	T_w, K	$\dot{m}$, $kg/m^2 \cdot s$	Rec rate, $\mu m/s$	$\dot{m}$, $kg/m^2 \cdot s$	T, K
1	282	98.3	20.0	11.6	0.190	170.6	0.0401	24.5	0.0392	177
2	280	99.3	29.4	12.3	0.187	170.6	0.0465	27.6	0.0441	a
3	280	99.0	24.3	12.3	0.187	170.6	0.0424	23.4	0.0371	182
4	274	97.7	38.3	9.5	0.177	170.0	0.0575	64.9	0.0396	185
5	273	97.7	28.0	11.9	0.176	170.0	0.0435	45.9	0.0285	182
6	277	97.0	24.6	12.4	0.182	170.2	0.0411	44.6	0.0273	183
7	276	98.5	21.4	11.8	0.180	170.3	0.0392	45.8	0.0284	a
8	276	98.5	21.3	10.2	0.180	170.3	0.0421	53.5	0.0332	a
9	279	97.7	18.6	10.1	0.185	170.4	0.0405	48.5	0.0296	179

[a]Temperature recording system failure. Runs 1–3 are pure carbon dioxide models. A temperature of 179 K was recorded on a pure model run with poor shape change results. Runs 4–9 are composite models. Other recorded asymptotic temperatures for composite models with poor shape change data are: 181 K, two at 182 K, 183 K, and 184 K.

below the amount predicted for pure carbon dioxide. The cause is not so easily explained. Conceptually, one could postulate that the cause was a reduction of heat transfer to the surface due to two-phase-flow effects in the boundary layer, some reduction due to subsurface events, or that the theoretical description of the surface events are inadequate. The obvious difference in final shape of the two materials suggests that the presence of glass beads did result in a heat-transfer distribution more similar to that of a turbulent boundary layer. However, the significant reduction in carbon dioxide mass flux prompted a more careful analysis of the surface. What follows is a more general analysis of the surface of the composite model, a discussion of the factors that can influence the mass loss, and an estimate of the magnitude in which these factors could have influenced the experiment.

Analysis of the Composite Material

Closer inspection of the idealized composite surface shown in Fig. 9 suggested that a new region be added to the analysis: the space between the subliming surface and the fluid dynamic wall above the beads. For this analysis, imagine that the control surface shown in Figs. 1 and 2 is now a control volume. A more complete treatment of this analysis is contained in Ref. 12. The more detailed treatment effects both the specie and energy conservation equations.

Specie Conservation Equation

The more detailed analysis shows that Eqs. (1) and (4) keep the same form but must be interpreted in a different way. In the simple theory the partial pressure of the subliming specie at the wall was assumed to be the equilibrium vapor pressure of the specie at the wall temperature. Now one must consider two new phenomena: 1) vapor passage through the glass beads which, at least in the stagnation region, might act as diffusion wells, attenuating the specie concentration, and 2) glass-bead blockage of a significant amount on the surface, causing locally high mass-transfer rates that would magnify the effects of nonequilibrium vaporization.

The first effect can be approximated using the result for evaporation through a simple, one-dimensional duct with constant area, temperature, and pressure.[17]

$$\frac{P-p_{1w}}{P-p_{1s}}=\exp\left[\left(\frac{\dot{m}}{F_D}\right)\frac{\ell RT}{DM_1P}\right] \tag{8}$$

The term F_D, the fraction of surface available for diffusion, has been added to increase the average mass flux to a value representative of the velocity in the well. The effect of this phenomenon, in conjunction with Eqs. (4) and (5), is to decrease B' and increase wall temperature.

Nonequilibrium effects, which cause the partial pressure of the subliming specie at the surface to be less than the equilibrium value, are modeled using the following equation:[3]

$$p_{1s}=(p_{1s})_{\text{eq}}-\frac{\dot{m}}{F_S\alpha}\sqrt{\frac{2\pi RT}{M_1}} \tag{9}$$

The term F_S adjusts the average mass flux for the lower fraction of total surface area actually available for sublimation. The effect of nonequilibrium sublimation is also a decrease in B' and an increase in wall temperature.[3,4] The glass beads increase the effect by causing locally higher mass flux through the surface.

Energy Equation

The effect on the conservation of energy equation is more obvious. Heat conduction paths through beads and gas wells give rise to a difference in temperature between the fluid dynamic wall and the subliming surface. The new equation is

$$B'=\frac{h_r-h_{2w}}{\Delta h_{\text{sub}}\left(1+\sum_{i=1}^{4}X_i\right)} \tag{10}$$

where

$$X_1=\frac{(\dot{q}_{\text{rad}})_{\text{net}}}{\dot{m}\,\Delta h_{\text{sub}}} \qquad X_2=\frac{\dot{m}^*(h_w^*-h_s^*)}{\dot{m}\,\Delta h_{\text{sub}}}$$

$$X_3=\frac{h_{1w}-h_{1s}}{\Delta h_{\text{sub}}} \qquad X_4=\frac{\dot{q}_{\text{int}}}{\dot{m}\,\Delta h_{\text{sub}}}$$

The nondimensional parameters X_i are the terms that were neglected in the earlier analysis. The definition of B' is the same.

Radiation heat transfer. The radiation heat-transfer contribution X_1 was approximately the same for both types of models, and, in any case, has only a percent or two effect on the final mass flux.

Solid material enthalpy gain. The spheres can heat up as they emerge from the subliming surface. They are exposed to the warmer air and they form islands that might not experience as much heat-transfer reduction due to vapor-phase mass addition to the boundary layer. Even if all of the heat is assumed to enter the model through the glass beads, the normalized effect on the energy equation X_2 is at worst a 1% effect.

Gas enthalpy gain. The gas temperature increases from the subliming surface to the fluid dynamic wall, but the normalized contribution X_3 is at worst a very small contribution.

Internal heat conduction. This term X_4 includes both transient and steady-state heat conduction. Since the thermal conductivity and thermal diffusivity of both models were nearly identical, this term should affect both in approximately the same way. The steady-state contribution for this experiment is negligible; however, in an experiment in which the predicted wall temperature has a large variation along the body, or if there is a large energy flux into the interior, the term should be retained. A transient heat-conduction analysis identified that this term could be significant, given a worst-case condition of an isothermal model suddenly exposed to the equilibrium wall temperature. This effect would decrease to a negligible value within 30 s. Since the internal heat flux is toward the surface, the result would be higher mass flux at the beginning of the experiment, which was not observed. In actuality, the transient processes probably began when the model was removed from the mold and had reduced to negligible rates soon after insertion into the airstream.

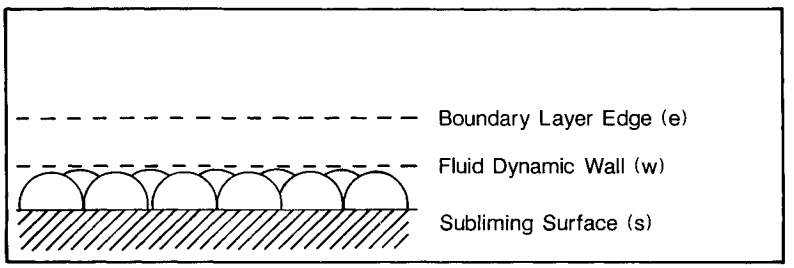

Fig. 9 Idealized view of ablating surface of composite material.

Results and Discussion

These effects were parametrically investigated using a computer model that coupled the more detailed equations. The geometrical parameters F_D and F_S were related to the well depth ℓ through an idealized geometric model of the surface. Although no complete explanation of the reduction was achieved, the factors that had the greatest effect on the mass flux were the diffusion well effect and amplification of the effects of nonequilibrium sublimation. Depths on the order of half of a bead diameter were large enough to affect the results. For nonequilibrium sublimation to be significant, the vaporization coefficient must be of order 0.001 or less, which could not be verified in the literature. Scala and Vidale[13] lists several of the known coefficients that vary from approximately 1 for water ice to 10^{-6} for red phosphorus. It is also known that the value of the coefficient is reduced at low temperatures. Although values lower than 0.001 are rare, they are not out of the question.

In extrapolation of these results to other systems, it is important to note that the major effects were a consequence of using a foreign material for the nonsubliming fraction. If the solid fraction is essentially the same material as the vaporizing material, such as the case with graphite, vaporization would then take place all over the surface, not just at the bottom of a well. Removal of solid particles would roughen the wall, which would increase the surface area available for vaporization rather than decrease it. In that case, little effect would be expected on wall temperature and vapor-phase mass flux. This work should serve as a warning to those who would deliberately seed an ablative material with a material that does not participate in the thermochemical process. Large amounts of nonvaporizing material can present resistance paths for diffusion of the vapor to the fluid dynamic surface and can aggravate the potential for nonequilibrium vaporization by causing locally high mass-transfer rates.

Conclusion

The effect of solid removal on the ablation process was investigated by comparing the ablation of pure carbon dioxide models to models with glass beads mixed with the carbon dioxide. The performance of the pure models was in close agreement to the predictions using rather simple thermochemical models. Extension of the simple theory to include the presence of solid removal predicted no change in the amount of vapor-phase mass transfer and the steady-state wall temperature. The experiments showed that the presence of glass beads reduced the carbon dioxide mass flux by 23% and caused a slight increase in steady-state surface temperature. In addition, there was a difference in the final shape of the composite models.

A more detailed theoretical model of the surface was developed. The ablating surface was replaced by a region between the subliming surface and the fluid dynamic wall. Although not completely explaining the experimental results, this model showed that the glass beads could cause the observed differences by either presenting diffusion paths for the vapor before it reached the fluid dynamic wall or reducing the amount of surface available for vaporization, aggravating the effects of nonequilibrium vaporization, or a combination of both phenomena.

Acknowledgments

This work was supported by the Air Force Institute of Technology and the Air Force Materials Laboratory of the Air Force Wright Aeronautical Laboratories, Air Force Systems Command. BLIMP results were run by Mr. Charles Powers, Aerotherm, Acurex.

References

[1]Kratsch, K. M., Martinez, M. R., Clayton, F. I., Greene, R. B., and Wuerer, J. E., "Graphite Ablation in High Pressure Environments," AIAA Paper 68-1153, Dec. 1968.

[2]Lundell, J. H. and Dickey, R. R., "Graphite Ablation at High Temperatures," *AIAA Journal*, Vol. 11, March 1973, p. 216.

[3]Baker, R. L., "Graphite Ablation Chemistry Non-equilibrium Effects," AIAA Paper 75-735, May 1975.

[4]Kubota, T., "Ablation With Ice Model at M = 58," *Journal of the American Rocket Society*, Vol. 30, Dec. 1960, pp. 1164–1169.

[5]Gazley, C., Gross, J., and Masson, D. J., "Mass Transfer Cooling in High-Velocity Flight," *Proceedings of the Third Symposium on High-Speed Aerodynamics and Structures*, Vol. 1, 1958, pp. 295–347.

[6]Kays, W. M., *Convective Heat and Mass Transfer*, McGraw-Hill, New York, 1966, p. 330.

[7]Lyon, C. A., "The Design and Construction of a Low Turbulence, Quiet, Free Jet Wind Tunnel," M.S. Thesis, U.S. Air Force Institute of Technology, Wright-Patterson AFB, OH, GAM/AE/73-3, 1973.

[8]Smith, A. M. O. and Pierce, J., "Exact Solution of the Newmann Problem. Calculation of Non-circulatory Plane and Axially Symmetric Flows about or within Arbitrary Boundaries." Douglas Co. Rept. ES 26988, April 1958.

[9]Bartlett, E. P. and Kendall, R. M., "An Analysis of the Coupled Chemically Reacting Boundary Layer and Charring Ablator. Part 3. Non-Similar Solution of the Multicomponent Laminar Boundary Layer by an Integral Matrix Method," NASA-CR-1026, June 1968.

[10]Maass, O. and Barnes, W. H., "Some Thermal Constants of Solid and Liquid Carbon Dioxide," *Proceedings of the Royal Society, A111*, 1926, pp. 224–244.

[11]Gotoh, K., "Thermal Conductivity of Two-Phase Heterogeneous Substances," *International Journal of Heat and Mass Transfer*, Vol. 14, April 1971, p. 645.

[12]Jumper, G. Y., "Thermomechanical Ablation," Dissertation, Air Force Institute of Technology, Wright-Patterson AFB, OH, DS/ME/75-1, Sept. 1975.

[13]Scala, S. M. and Vidale, G. L., "Vaporization Process in the Hypersonic Laminar Boundary Layer," *International Journal of Heat and Mass Transfer*, Vol. 1, No. 1, 1960, pp. 4–22.

[14]Giauque, W. F. and Egan, C. J. "Carbon Dioxide, The Heat Capacity and Vapor Pressure of the Solid. The Heat of Sublimation. Thermodynamic and Spectroscopic Values of the Entropy," *Journal of Chemical Physics*, Vol. 5, Jan. 1937, pp. 45–54.

[15]Eckert, E. R. G. and Drake, R. M., Jr., *Heat and Mass Transfer*, McGraw-Hill, New York, 1959, pp. 493ff.

[16]Brown, G. G. et al., *Unit Operations*, Wiley, New York, 1955, p. 214.